Copper abundances of F and G dwarf stars in the Milky Way

Filip Andersson

Lund Observatory
Lund University

2017-EXA108

Degree project of 15 higher education credits
January 2017

Supervisor: Thomas Bensby

Lund Observatory
Box 43
SE-221 00 Lund
Sweden

Abstract

An investigation has been done in order increase the understanding of the origin and chemical evolution of copper in the Milky Way stellar disks. This is interesting to know as it plays a part of the Galaxy puzzle, so we become more able to map how and why galaxies look like they do.

The atmosphere of a star keeps information about how elemental abundant the Universe was at the time and place of creation, as the atmosphere remains intact during its lifetime. Dwarf stars with their long lifetime of billions of years may in other word keep information about the early days of our Universe. So, by determining the copper abundances for 502 F and G dwarf stars in the Solar neighborhood of different age, the evolution of copper can be determined. The copper abundance was measured through comparisons of synthetic spectra, with different copper abundances, to observed spectra, where the spectrum with the best fit was chosen.

The star sample was a compound of different observations. Mainly, the stars were chosen to trace and characterize the thin and thick disks in the Solar neighborhood. The stars were observed with the MIKE spectrograph on the Magellan Clay telescope.

491 out of these 502 stars were able to give results good enough to be taken into account. When the result was normalized to the Sun, it was found out that the copper abundance, of this star sample, ranges between $-0.6 < [\mathrm{Cu/Fe}] < 0.2$ dex, while the metallicity for the star sample ranges between $-1.7 < [\mathrm{Fe/H}] < 0.4$ dex. A rising copper abundance trend is seen in the metallicity range $-1.7 < [\mathrm{Fe/H}] < -0.6$ dex, with a flat area between $-0.6 < [\mathrm{Fe/H}] < 0$ dex. For $[\mathrm{Fe/H}] > 0$ a rising trend is once again seen. This rising trend for the copper abundance supports the idea that copper comes from both type II supernovae, and that the contribution of copper is metallicity dependent. The flat trend supports the idea that copper is made in type Ia supernovae.

Populärvetenskaplig beskrivning

Metalliciteten hos en stjärna är den del av materien som inte består av helium eller väte. Detta innebär att när en astronom talar om metallicitet, inkluderar hon även icke-metalliska grundämne, såsom kol, syre eller något av de tyngre grundämnena. Genom att studera metalliciteten hos en stjärna kan vi lära oss en del om dem, till exempel dess ålder och ursprunget för var våra grundämnen kommer ifrån.

Målet med detta projekt är att ta reda på vart, i universum, koppar kommer ifrån. Olika teorier finns, där en del pekar på att det är supernovor av typ Ib, Ic och II och andra menar på att koppar kommer ifrån exploderande vita dvärgar, det vill säga supernovor av typ Ia. Det finns även de som hävdar att koppar uppstår från s-processen, den långsamma neutroninfångande process.

Spektroskopi är en metod som kan användas för att observera en stjärnas spektrum. Ett spektrum är när ljuset är uppdelat i olika våglängder och för att göra detta kan man använda sig av en prisma eller, ännu vanligare i astronomi, ett gitter, där ljus reflekteras och beroende av våglängd, reflekteras i olika vinklar. I ett spektrum är det de olika grundämnena som ansvarar för de olika spektrallinjerna i spektrumet. Detta innebär att med en stjärnas spektrum kan många saker bestämmas, till exempel temperatur, massa, densitet och det vi är ute efter, metallicitet.

I detta projekt har kopparymnigheten bestämts för 502 dvärgstjärnor av typ F och G i solens närhet. Detta gjordes genom att skapa syntetiska spektra, som anpassades till det observerade spektrummet. Då kopparymnigheten ansvarar för hur intensiva spektrallinjerna är, kan ymnigheten bestämmas på detta sätt. Av alla observerade stjärnor var det 491 stjärnor som gav result bra nog att presenteras. Det solnormaliserade kopparymnightsresultatet sträcker sig mellan $-0.6 < [\mathrm{Cu/Fe}] < 0.2$ dex och de stödjer teorier för att koppar uppstår från typ II och Ia supernovor, samt s-processen då lågmetallicitetsstjärnorna och är metallicitetsberoende.

Contents

Chapter 1

Introduction

With the common goal to unveil how galaxies are formed and the chemical evolution of the galaxies, this thesis will take a closer look at the origin and evolution of copper in the Solar neighborhood. As the atmospheres of low-mass F and G dwarf stars remain intact over the life times of the stars, their spectra can be used to track the chemical abundance in the gas cloud, which formed the star billions of years ago. The sample, which contains 502 F and G type dwarf stars, becomes a good sample since the expected main sequence of these kinds of stars is about as long, or longer, than the age of the Milky Way itself. Through synthesizing spectra of stars, with different amounts of copper, and by applying the synthetic spectra to the observed spectra of the stars, the copper abundances can be determined.

1.1 Background

In the point of view of an astronomer all elements that are neither hydrogen nor helium are considered to be metals. This fraction is called the metallicity which hereby includes elements which on earth does not fulfill the properties to be a metal, for example nitrogen (N) and carbon (C). Although oxygen (O) is generally the third most abundant element in stars, iron (Fe) is used to measure the metallicity. This is due to Fe being the easiest element to achieve spectral data from in the visible spectrum due to the atomic structure of Fe.

In order to understand the chemical evolution, we must first understand what processes that are responsible for the nucleosynthesis of interest. In metal-poor stars Sneden & Crocker (1988); Sneden et al. (1991) and Matteucci et al. (1993) say that copper is produced from the weak component in the slow neutron capture process (s-process). This process occurs when free neutrons and an element react in a β-decay to create a new element. Free neutrons become available due to the alpha process where the most common reaction is ${}^{13}_{6}\mathrm{C} + {}^{4}_{2}\mathrm{He} \rightarrow {}^{16}_{8}\mathrm{O} + \mathrm{n}$. The reason this process is called slow is due to the relatively low neutron flux where years may pass in between neutron catches and the entire process lasts for thousands of years.

Sneden & Crocker (1988); Sneden et al. (1991) and Matteucci et al. (1993) says that

another source of copper nucleosynthesis is type II supernovae. Stars with masses greater than 8 solar masses ($M_\odot$) but less than 50 $M_\odot$ possess enough mass to fuse elements heavier than helium (Gilmore (2004)). This increases the temperature and pressure as well as it shortens the life time of the star drastically, giving stars of this size only millions of years life-time. However, the mass of the star is only big enough to fuse elements up to iron and nickel, and thereafter the fusing becomes endothermic which cannot maintain the pressure outwards. When the core of iron reaches the Chandrasekhar limit, 1.4 $M_\odot$, the electron degeneracy pressure is no longer able to support its weight and the core implodes, rebound and bounce outwards creating a shock wave. The force of the shock wave is strong enough so that the outer layers of the star reach the escape velocities. This shock wave reaches temperatures and pressures that allow the elements heavier than iron and nickel to be produced. Due to the average low life time of the stars of this size one can consequently understand that in the early days of the universe supernovae type II were dominant compared to other types of supernovae.

Another big source of copper nucleosynthesis is type Ia supernova (Matteucci et al. (1993), Romano & Matteucci (2007) and Mishenina et al. (2002)). These kinds of supernovae come from binary systems of stars where one of them must be a white dwarf while the other can be anything from a smaller white dwarf to a giant star. The white dwarf gains mass from its companion star until the white dwarf reaches the Chandrasekhar mass limit and, due to the same reason as before, implodes and the rebounding shock wave causes the explosion.

1.2 Aim of this work

To know the origin of all elements increases the understanding of how stars and galaxies are created, since all elements, except for hydrogen and helium, are produced in stars in different ways. Some are created during the stars' lifetimes, some are created while stars die and a few are created from remnants of dead stars. In this thesis, the focus lies on copper (Cu) which is an element with a spectrum that is harder to observe than for example iron (Fe) due to the atomic structure of each element. The stars used in this thesis come from Bensby et al. (2014), where the abundance of several elements (e.g. Fe, oxygen (O), magnesium (Mg) and aluminum (Al)) are measured for the same spectra.

The spectrum of a star can tell us much about it, e.g. the temperature, the mass and the chemical composition. This thesis will use spectra of 502 F and G dwarf stars in the Solar neighborhood, where synthesized spectra will be created and compared to the observed spectrum and the one with an abundance that best fits the observed spectrum will be chosen as the copper abundance of that specific star. The reason that this time consuming synthesizing spectra method will be used instead of the measuring the equivalent width, is due to the hyperfine structure of copper, since it is an odd Z iron peak element. The reason that elements with odd number of electrons suffer more from hyperfine structure is due to that when the resultant angular momentum $J > 0$ and the spin of the nucleus $I > 0$ magnetic dipole and quadrapole occurs (Schwartz (1955)). This means that copper does not consist of one spectral line, but many spectral lines, which in turn ruin the Gaussian

shape of the spectral line.

The star sample, used in this thesis, is the same subset of stars that are used by Bensby et al. (2014). The sample selection comes from different observing campaigns with different aims. However, the most important aim was to characterize the thin and thick disks in the Solar neighborhood. More details on how and why these stars were selected can be found in the article by Bensby et al. (2014).

1.3 Theory

To understand the spectrum of a star it requires that one understands the nature of the atmosphere of the star. The atmosphere is defined as the transition from the interior of the star to the interstellar medium. For the observer, the spectrum mainly originates from the photosphere, which is the part of the atmosphere that is closest to the "surface" of the star (Gray 2008). The first thing to take into account, that strongly affects the geometrical extent of the photosphere, is the surface gravity, g.

$$g = g_{\odot}\frac{M}{R^2} \tag{1.1}$$

where $g_{\odot}$ is the surface gravity of the Sun ($2.740 \cdot 10^2$ m/s^2). M is the mass, and R is the radius of the star, both given in Solar units.

The second parameter that affects the nature of the photosphere is the effective temperature, T_{eff}, as it varies with a factor of two from the bottom to the top of the photosphere. The effective temperature is defined in terms of the total power per unit area radiated by the star,

$$\int_0^{\infty} F_{\nu}\, \nu = \sigma T_{eff}^4 \tag{1.2}$$

where F_{ν} is the flux leaving the stellar surface and $\sigma = 5.670$ erg/(s cm^2 deg^4).

Small-scale mass motions where the characteristic dimensions of the moving material are small compared to the unit optical depths are called microturbulence, ξ (Gray 2008). These phenomena produce Doppler shifts that are equivalent to those arising from thermal motion, which means that there will be an absorption coefficient where microturbulence will affect the Doppler broadening:

$$\Delta\lambda_D = \frac{\lambda_0}{c}\left(\frac{2kT}{m} + \xi^2\right)^{1/2} \tag{1.3}$$

Here $\Delta\lambda_D$ is the line broadening around wavelength λ_0 and c is the speed of light. k is the Boltzmann constant and T is the temperature, which in our case $T = T_{eff}$ and m is the mass of the atom.

The metallicity is defined by:

$$[Fe/H] = log[A(Fe)/A_{\odot}(Fe)] \tag{1.4}$$

where $A(Fe)$ is the abundance of the star and $A_{\odot}(Fe)$ is the abundance of the Sun.

Chapter 2

Method

For this thesis, the abundance determination will be done by comparing synthesized spectra to the observed spectrum. The reason for this method to be used is due to the hyperfine structure of copper, which ruins the Gaussian shape of the spectral lines.

The atmosphere for the synthetic spectra will use a standard local thermodynamic equilibrium, LTE, which is one dimensional and plane parallel. There is LTE when temperature and heat exchange change slowly enough for one to assume thermodynamic equilibrium of the point of interest. The model atmospheres were calculated with the MARCS code (Gustafsson et al. 2008).

2.1 Copper lines

Copper has two stable isotopes ^{63}Cu and ^{65}Cu, where ^{63}Cu is the more abundant one, contributing about 69% of the total Cu abundance in the Solar System (Simmerer et al. 2003). Copper is also said to belong to the odd-Z element iron peak. This means that copper lines contain hyperfine splitting. Hence, copper suffers significantly from broadening effects and the line profiles are not Gaussian in shape. This can be seen in Fig. 2.2 where the wavelength of the hyperfine components are marked with black vertical lines.

In Simmerer et al. (2003) the line 5105.5 Å was used as it is strong enough to be observed in metal-poor stars. However, Simmerer et al. (2003) also say that this line is an intrinsically stronger transition, relative to other copper lines, and will be less reliable as the metallicity increases. This is the reason why this spectral line was chosen to be a part of this thesis. However, the line faces the problem that it is located in a crowded area of the spectrum. Several MgH features lie near 5100 Å and become quite strong in cool and metal-rich stars. This makes it difficult to find continuum points around this area of the spectrum.

5218.2 Å was also chosen to be a part of this thesis due to the strength of the spectral line combined with the uncrowded area, which made it easy to determine the continuum points. Yan et al. (2016), used this spectral line to measure the copper abundance in two distinct halo populations in the Solar neighborhood.

The third spectral line to be a part of this thesis is the one at 5782.1 Å. This spectral

line is also used by Simmerer et al. (2003), using the same argument as for the 5105.5 Å line, that this line is strong enough to be useful for metal poor stars.

According to Yan et al. (2016), who used all three spectral lines as in this thesis, stars with low metallicity, suffer significantly from non-local thermodynamical equilibrium, NLTE (up to 0.2 dex). However, this thesis does not take NLTE to account.

2.2 Atomic Line Data

Atomic line data, needed for the synthesizing spectra, is taken from Vienna Atomic Line Data, VALD3, and hyperfine structures, around the chosen spectral lines, are taken from the article by Prochaska et al. (2000). These data provides parameters for elements around the spectral line of interest. The parameters used from here are type of element, wavelength and oscillator strength (log gf). These data can be seen in appendix A.1, A.2 and A.3.

2.3 Stellar Sample and Parameters

The stellar sample incorporate F and G dwarf stars in the thin disk and thick disk, and only a few in the halo in the Solar neighborhood in the Milky Way. These stars are the same subset of stars that are used by Bensby et al. (2014), who obtained the spectra with the MIKE spectrograph on the 6.5 m Magellan telescopes at Las Campanas, Chile. The spectral resolving power are $R = 42000$, $R = 55000$ or $R = 65000$, depending on what different slits were used, with a high signal to noise ratio which is generally around or above 250.

The stellar parameters for the star sample are derived in Bensby et al. (2014) and for more details I suggest reading this article. In summary: The effective temperature is calculated by using the excitation balance of the Fe I lines. The surface gravity is calculated by using the ionization balance between Fe I and Fe II.

2.4 Line Synthesis

In order to determine the copper abundance, one can synthesize spectra to fit the observed spectrum to find the abundance with the best fit. For each observed spectrum, ten synthetic spectra were created, with set effective temperature, micro turbulence, surface gravity, metallicity, macro turbulence, log gf and varying copper abundances. The combined line broadening due to macro turbulence and $\nu sini$ was estimated by analyzing three lines of iron at 6065 Å, 6546 Å and 6678 Å at the same time. The difference in between each synthetic spectrum and the observed spectrum was calculated, and the abundance with the smallest uncertainty in $\sum \chi^2$ was chosen to be the starting point for the next set of synthetic spectra. An example of this can bee seen in Fig. 2.1 In Fig. 2.1a the synthetic spectra and observed spectrum are shown, in Fig. 2.1b one can see the difference in intensity, and in Fig. 2.1c, $\sum \chi^2$ are plotted against copper abundance. Next, an

additional ten spectra were created and the copper abundances now varied in smaller steps. In this finer analysis, the abundance was also measured with varying uncertainty parameters to find the copper abundance with varying uncertainty. These uncertainties were the surface temperature of the star (effective temperature T_{eff}), log g, metallicity ([Fe/H]) and micro turbulence (ξ) where one parameter was calculated at a time, and also the upper limit and lower limit for each parameter was done, one at a time. These values were then used to calculate the total uncertainty with Eq. 2.2

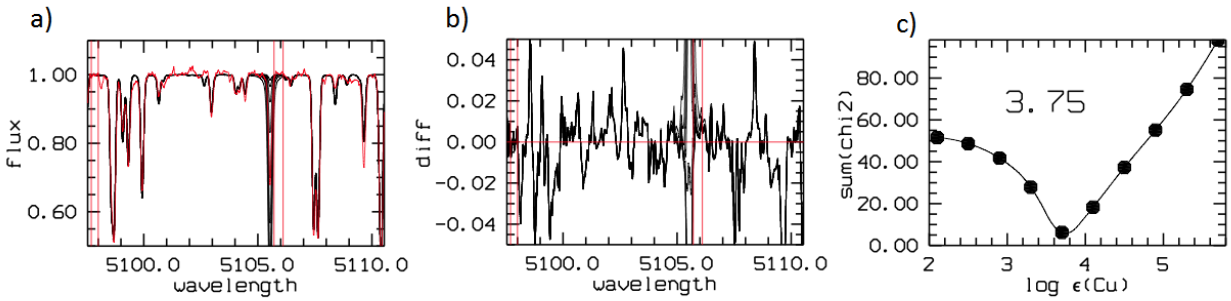

Figure 2.1: Figures of how the first step of the analysis could look. This is for star HIP 54469. In a) we see the intensity flux versus the wavelength. Here the observed spectrum is red and the synthetic spectra are black. In b) we once again see the intensity flux versus wavelength, but now we see the difference between the observed spectrum and the synthetic spectra. In c) we see $\sum \chi^2$ versus the copper abundance, $log\,\epsilon(Cu)$.

Spectroscopy Made Easy, SME, is a software for the programming language IDL. SME has an external library and is created for fitting spectra with high resolution with synthetic spectra to determine stellar parameters. To learn more about SME, look at the work by Valenti & Piskunov (1996).

In this thesis a script, written in ESO-MIDAS language, was used as a wrapper around SME, and contained the fitting routines. MIDAS initiates SME with a set of parameters and then fits the observed spectrum with different analytical spectra. Here, the script took into account the wavelength shift, due to the Doppler shift, which occurs due to the relative velocity away or towards the observer. Then the continuum of the spectra were set by taking the median of two different line regions of the same spectrum, one with lower and one with higher wavelength then the spectral lines. The continuum intervals were set manually in the script. The script then calculated the difference between the synthetic spectra and the observed spectrum and chose the synthetic spectrum with lowest difference as the best fit. This was done by taking the sum of the squares, $\sum \chi^2$, then taking the synthetic spectrum, and do a refined analysis. The refined analysis used smaller abundances steps of 0.06 dex, around the old best value to increase the fit for the spectrum. Then the new abundance with lowest $\sum \chi^2$ was used as the copper abundance of the star. An example of the final result can be seen in Fig. 2.2 where the results of all three spectral lines are shown.

2.5 Solar Copper Abundance

The solar abundance has also been measured so that systematic errors, which can occur when using the solar abundance from someone else, will be as low as possible. The same method as before was used to determine the solar copper abundance. For each spectral line, the average of the logarithmic result was subtracted from each stellar result to get values that are normalized to the Sun, see Eq. 2.1. Then the average was taken from the three lines. The reason this is done, is to normalize the result with the Sun so that the result can be compared to other abundances studies. This normalization is calculated with Eq. 2.1 where N is the number density of each respective element.

$$\left[\frac{Cu}{Fe}\right] = log\left(\frac{N_{Cu}}{N_{Fe}}\right)_{\star} - log\left(\frac{N_{Cu}}{N_{Fe}}\right)_{\odot} \tag{2.1}$$

Solar parameters were taken from the work by Bensby et al. (2014), which were $T_{eff} = 5773$ K, $\log g = 4.42$, $\xi_t = 0.88$ km s^{-1} and $\log \epsilon(\mathrm{Fe}) = 7.58$. The solar spectra were recorded by observations of the reflection from Ganymede, one of the moons of Jupiter, and the asteroid Ceres. The spectra from these were also from the same observations as in Bensby et al. (2014).

2.6 Uncertainties

Copper is an element that is dependent on the metallicity, surface gravity, effective temperature and micro turbulence of a star. With the uncertainty of these parameters in the article by Bensby et al. (2014) an additional eight different synthesized spectra were produced for each spectral line where these parameters were varied. The final uncertainty was calculated with this formula:

$$\Delta A = \sqrt{\Delta A^2_{T_{eff}} + \Delta A^2_{log\, g} + \Delta A^2_{[Fe/H]} + \Delta A^2_{micro}} \tag{2.2}$$

where $A \equiv \log \epsilon(\mathrm{Cu})$ is the absolute abundance of copper. Where the definition of the absolute copper abundance is:

$$log\, \epsilon(Cu) \equiv log\left(\frac{N_{Cu}}{N_H}\right) + 12.0 \tag{2.3}$$

where N is the number density of each respective element.

Another uncertainty that occurred was where the continuum was set. If the continuum is misplaced, the entire continuum will tilt, giving a misleading size of what the spectral line really looks like. For the spectral line at 5105 Å this was a problem due to the populated area around spectral line, as earlier stated, the MgH lines. This uncertainty is not taken to account in the final result.

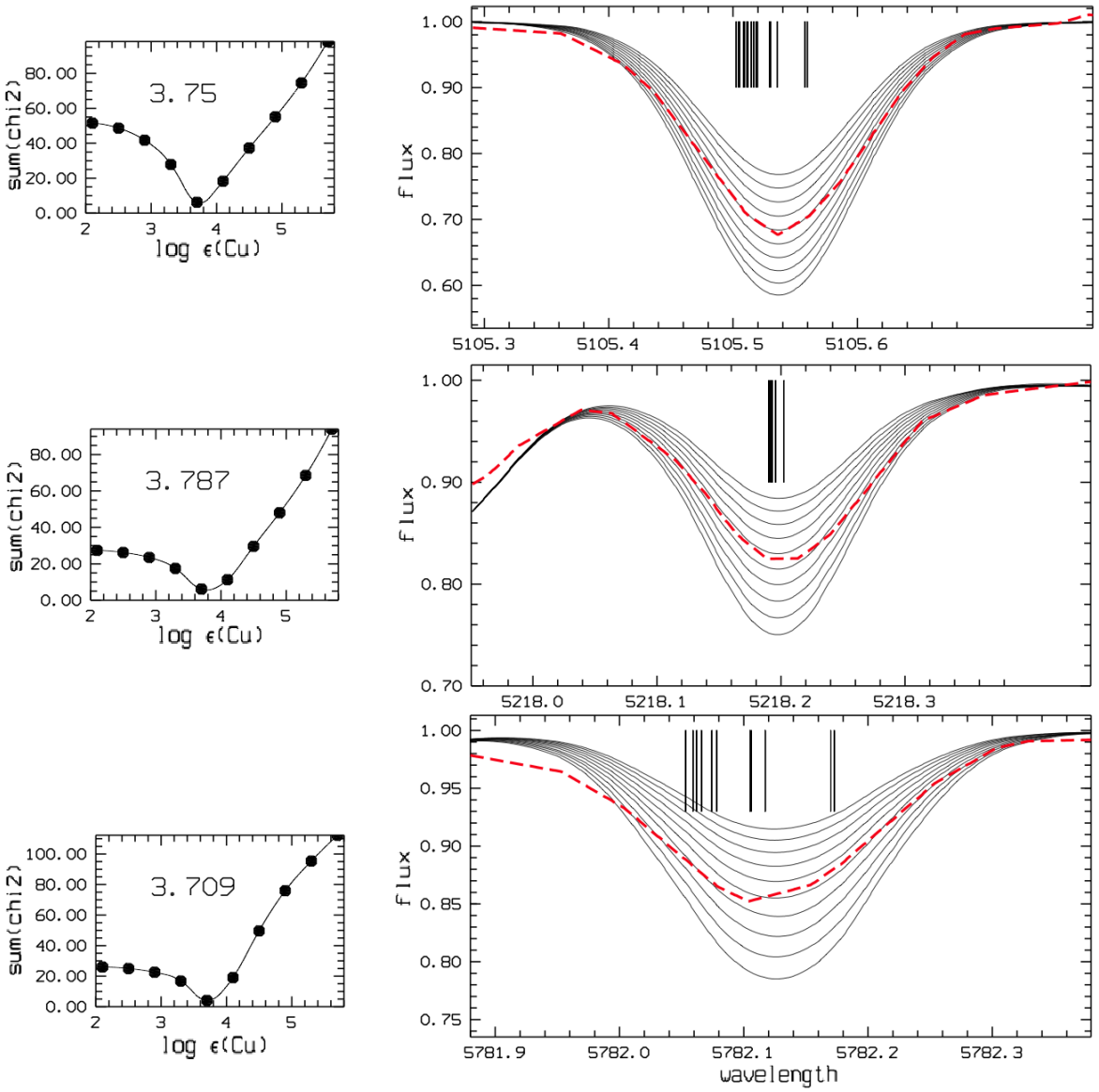

Figure 2.2: These plots are examples of the results. To the left we see the sum of the squares, $\sum \chi^2$, and to the right the black lines are the synthesized spectra while the red dotted lines represent the observed spectrum of star HIP 54469. The black vertical lines represent the hyperfine lines for copper at each respective spectral line. a) For the spectral line at 5105 Å we have a total of 17 hyperfine lines. b) For the spectral line at 5218 Å we have a total of 17 hyperfine lines. c) For the spectral line at 5782 Å we have a total of 11 hyperfine lines.

Chapter 3

Results and discussion

3.1 Abundances

3.1.1 Solar Abundances

In table 3.1 we see the solar copper abundance used to normalize the stellar abundances. All of the results lie close to each other, but one can see that the abundance for the spectral line at 5782 Å is a little bit lower than the others. This feature is seen for the other stars as well, as can be seen in Fig. 3.1.

The overall copper abundance measured in this thesis, lies a bit below what was measured by Asplund et al. (2005) where the copper abundance was measured to be 4.21 $\pm$ 0.04.

Table 3.1: shows the solar copper abundances. The number after the observed object only represents observing run.

Observed object	log ϵ(Cu) (5105 Å)	log ϵ(Cu) (5218 Å)	log ϵ(Cu) (5782 Å)
Ceres 1	4.232	4.150	4.076
Ceres 2	4.215	4.148	4.052
Ceres 3	4.231	4.147	4.072
Ganymede 1	4.189	4.160	4.050
Ganymede 2	4.164	4.135	4.081
Average	4.206	4.148	4.066

3.1.2 Abundances from the Different Lines

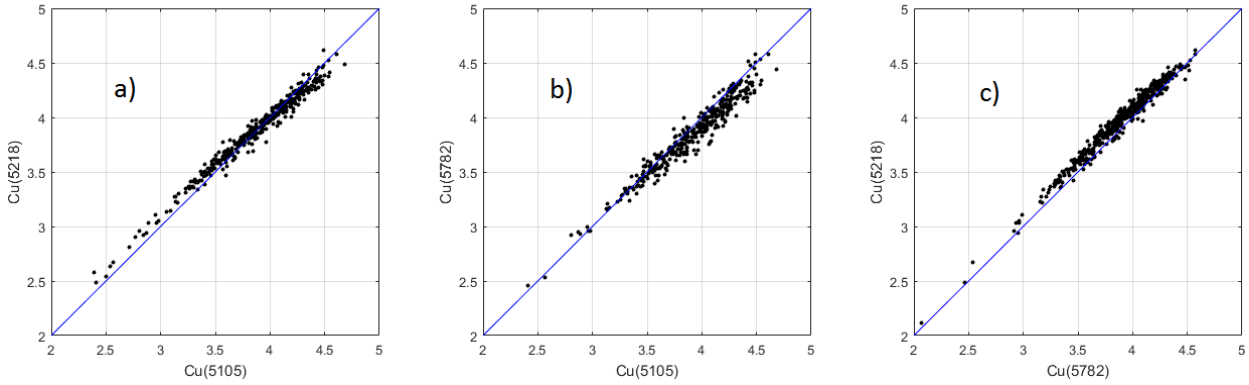

Figure 3.1: Plots of the absolute copper abundance compared with other lines. a) 5105 Å versus 5218 Å. b) 5105 Å versus 5782 Å. c) 5782 Å versus 5218 Å.

By looking at the plots in Fig. 3.1 we see that the consistency is very good for stars with lower metallicity but starts to deviate more as the copper abundance goes up. The exception is for Fig. 3.1a where the 5218 Å. seems to be constantly stronger for low metallicity stars. It also appears that the spectral line at 5782 Å tends to give a lower results than the other two spectral lines. Results have been sorted out in a way so that the lines, where the synthetic spectra could not be fit into the observed spectrum, are removed.

There were a total of 98 stars where the 5105 Å spectral line where the synthesized spectra were too far off the observed spectrum to be accepted as a good results. The stars are present in appendix B.1. What one can see from this is that stars with a [Fe/H] that is around 0 dex or above, have a higher risk of giving bad result for this spectral line. Also, for stars that have a metallicity around and below -1.6 are too low to measure with this spectral line.

For the spectral line at 5218 Å, a total of 18 stars gave bad result. These stars are present in appendix B.2. These are generally stars with a metallicity of around -1.6 dex or below.

There were a total of 37 stars where the spectral line 5782 Å could not achieve results that were good enough. These stars are present in appendix B.3. The difference between this line and the line at 5218 Å is the strength of the line since it looks like there are problems achieving good results around -0.8 dex and below.

As the three different spectral lines gave different result it could be interesting to see if this could be due to the metallicity, effective temperature or surface gravity. To check this difference in copper abundance, each respective spectral line was taken and plotted against these parameters. This can be seen in Fig. 3.2, 3.3 and 3.4.

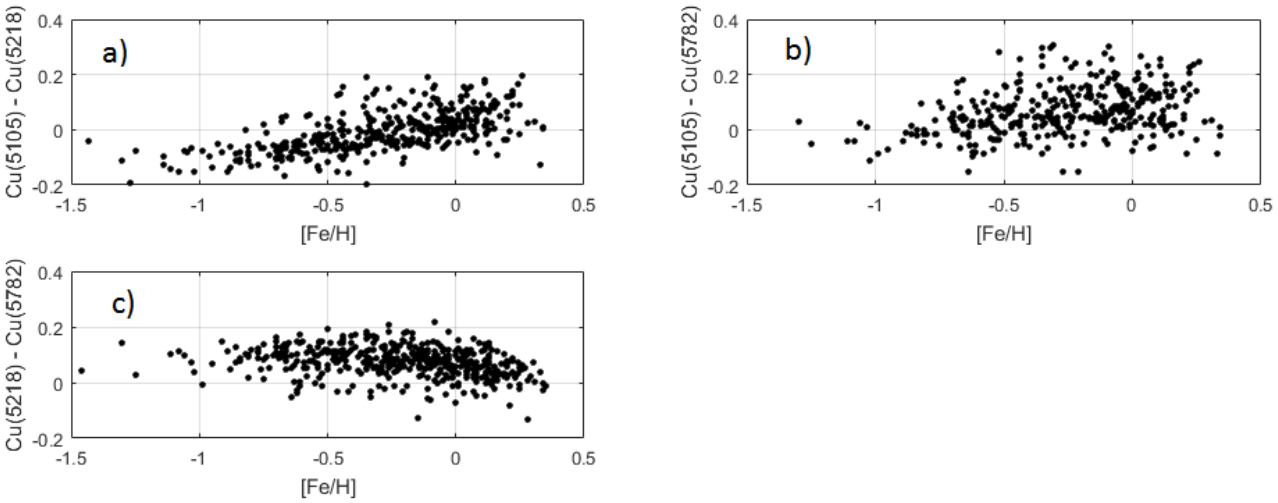

Figure 3.2: Plots of the difference in copper abundance, between each spectral line versus metallicity. a) Cu(5105)−Cu(5218) versus [Fe/H]. Cu(5105)−Cu(5782) versus [Fe/H]. c) Cu(5218)−Cu(5782) versus [Fe/H].

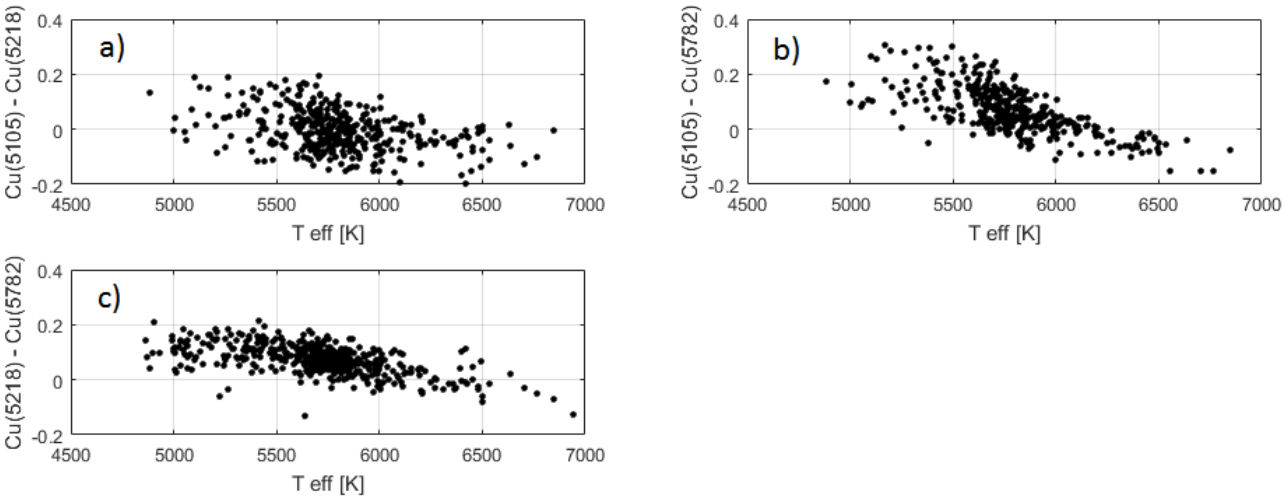

Figure 3.3: Plots of the difference in copper abundance, between each spectral line versus effective temperature. a) Cu(5105)−Cu(5218) versus T_{eff}. Cu(5105)−Cu(5782) versus T_{eff}. c) Cu(5218)−Cu(5782) versus T_{eff}.

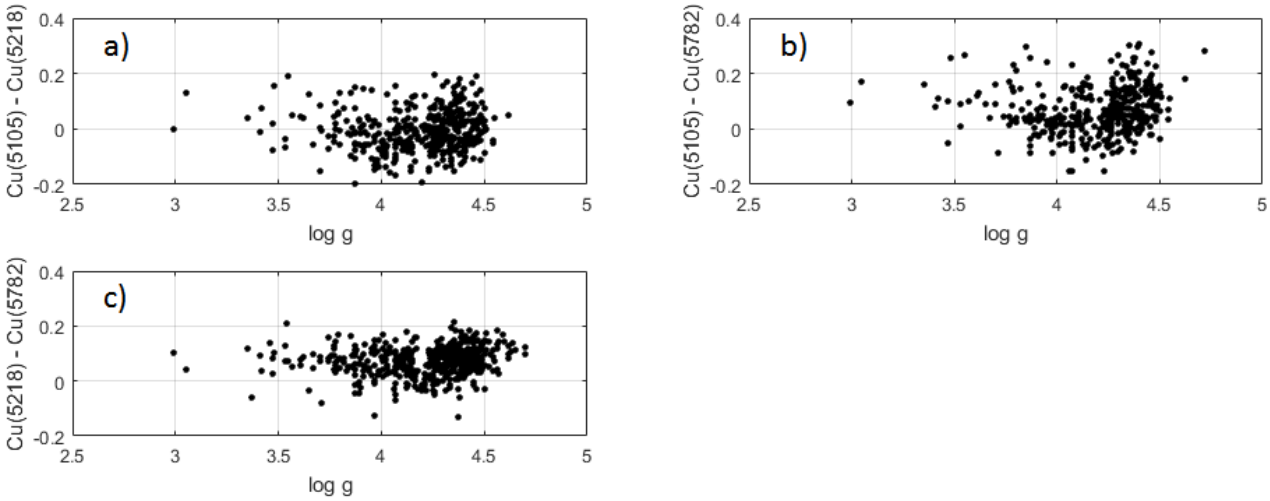

Figure 3.4: Plots of the difference in copper abundance, between each spectral line versus the surface gravity. a) Cu(5105)−Cu(5218) versus log g. Cu(5105)−Cu(5782) versus log g. c) Cu(5218)−Cu(5782) versus log g.

In Fig. 3.2 the copper abundance differences between the spectral lines are plotted against the metallicity In Fig. 3.2a and 3.2b one can see a rising trend, meaning that the results, for spectral line 5105 Å, are relatively affected due to the metallicity of the star. In Fig. 3.2c we see that spectral line 5218Å seems to be constantly 0.1 dex stronger than spectral line 5782 Å when [Fe/H] < 0. As the metallicity becomes higher the 5782 Å becomes stronger in both Fig. 3.2b and 3.2c.

In Fig. 3.3 the copper abundance difference between the spectral lines are plotted against the effective temperature. All three sub figures display flat areas for $T_{eff} < 5500$ where the line, which is theoretically stronger, appears to give a higher result. As the temperature increases, the weaker lines gives relatively higher result, which results in decreasing trends in all three plots.

In Fig. 3.4, where the copper abundance difference of the spectral lines are plotted against the surface gravity, there does not seem to be any particular trends. One might however argue that there is a rising trend at log $g > 4$.

To make this comparable to why the values for the Sun deviate, Tab. 3.2 was created. Here, the average at each line has been taken under different parameter intervals. One can see that it appears that the metallicity is most responsible for the abundance deviation for each line. However, the differences are still much higher for the Sun.

Table 3.2: shows the average differences in copper abundance for the different lines. The left column shows which stars are taken into account in the average. The parameter interval is chosen in such a way so the stars have that specific parameter close to the Solar value. "All 3 Fulfilled" means that only stars which can fulfill all three intervals are taken to account.

Parameter (interval)	Cu(5105)−Cu(5218)	Cu(5105)−Cu(5782)	Cu(5218)−Cu(5782)
[Fe/H] (−0.2 to 0.2)	$2.9 \cdot 10^{-2}$	$8.8 \cdot 10^{-2}$	$6.7 \cdot 10^{-2}$
T_{eff} (5500 to 6000 K)	$-7.4 \cdot 10^{-3}$	$6.7 \cdot 10^{-2}$	$7.7 \cdot 10^{-2}$
log g (4.2 to 4.6)	$3.3 \cdot 10^{-4}$	$7.5 \cdot 10^{-2}$	$7.8 \cdot 10^{-2}$
All 3 Fulfilled	$2.7 \cdot 10^{-2}$	$9.3 \cdot 10^{-2}$	$6.8 \cdot 10^{-2}$
All Star sample	$-7.4 \cdot 10^{-3}$	$6.7 \cdot 10^{-2}$	$7.4 \cdot 10^{-2}$
The Sun	$5.8 \cdot 10^{-2}$	0.14	$8.2 \cdot 10^{-2}$

Out of the 502 stars that were measured, there were 11 stars of which none of the chosen spectral lines were able to achieve results good enough to use. They are presented in table 3.3. As one can see all of these stars have low metallicity of around −1.6 dex or lower.

Table 3.3: shows the stars that are removed due to no spectral line capable of achieving results that are good enough.

Id of star (HIP)	[Fe/H] (dex)	T_{eff} (K)
8572	-2.62	5931
36269	-1.66	6152
60632	-1.75	6140
68464	-1.82	6043
76976	-2.62	5658
86694	-1.85	5986
88010	-1.34	5424
89554	-1.57	6229
93186	-2.31	5966
114761	-0.65	6712
114962	-1.50	5935

In table 3.3 we can see that HIP 88010 and HIP 114761 do not have as low metallicity as the other stars in the table. The reason that these stars have bad results is unfortunately due to disturbance in the observed spectrum at the spectral lines of interest.

It is also worth to mention what could happen if NLTE was applied to the measurement. According to Yan et al. (2015) the three lines, used in this thesis are differently affected by NLTE. The result for spectral lines at 5105 Å and 5782 Å could affect the result as much as 0.2 dex, while 5218 Å is not that sensitive, but still not negligible, about 0.13

dex. This paper concludes that copper is under abundant in LTE environment. NLTE effects are also metallicity dependent, affecting the result metal-poor stars more.

3.1.3 Copper abundance for different stellar parameters

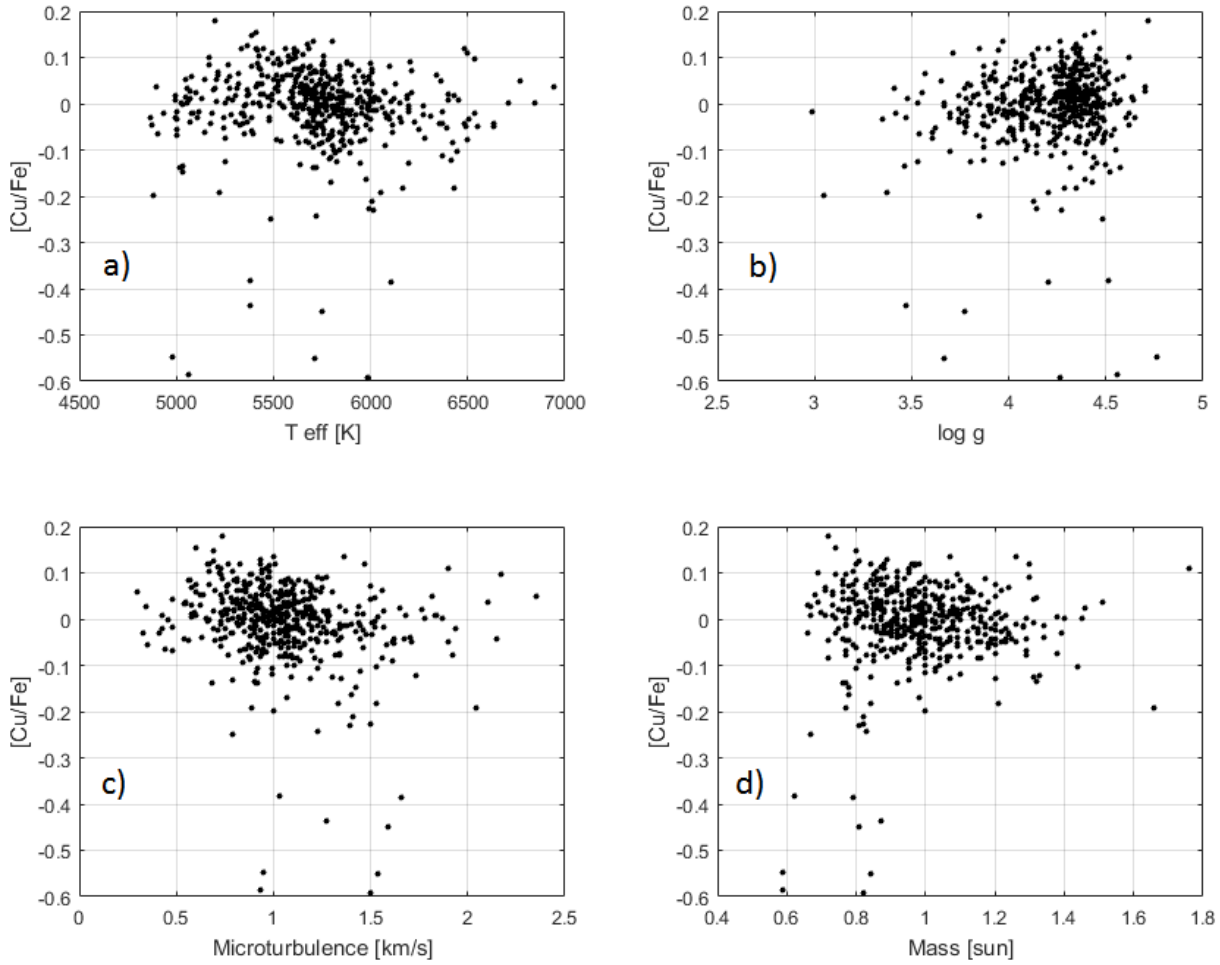

Figure 3.5: Plots of copper abundance versus various interesting stellar parameters: a) the copper abundance versus effective temperature. b) the copper abundance versus surface gravity. c) copper abundance versus micro turbulence. d) copper abundance versus mass.

The final result is now calculated as the mean average for the three spectral lines. In Fig. 3.5 the copper abundance versus the effective temperature, surface gravity, micro turbulence and mass can be seen. There are no particular trends in any of the cases. The copper abundance does, in other words, not depend on neither the effective temperature,

surface gravity, micro turbulence nor the mass of the star. There are a few stars with low copper abundance, these stars are older and belong to the thick disk/halo.

3.1.4 Copper abundance versus metallicity

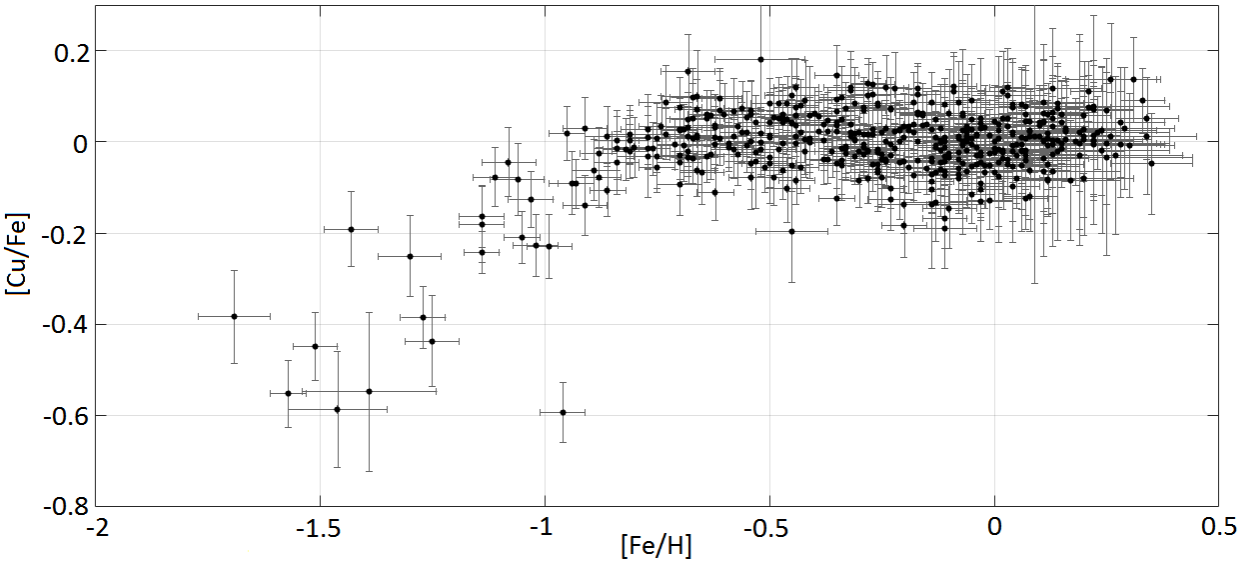

Figure 3.6: A plot that shows copper abundance versus metallicity with error bars.

In Fig. 3.6 we can see the copper abundance versus the metallicity where the uncertainty in copper abundance is shown. The uncertainty in [Cu/H] was calculated using the formula in Eq. 2.2 and the uncertainty for [Fe/H] is taken from Bensby et al. (2014). To get the uncertainty in [Cu/Fe] the uncertainties from [Cu/H] and [Fe/H] were added in quadrature. In the plot the entire star sample is shown. For further simplicity and clarity in the plots, error bars will not be used for the later plots.

As we can see in Fig. 3.6 there is a slope in the the metal-poor region of [Fe/H] < -0.6 dex. While, in the higher metallicity regime, [Fe/H] > -0.6 dex, the abundance is more or less constant around [Cu/Fe] $= 0$ dex. According to Cunha et al. (2002) this rising behavior for [Fe/H] < -1, makes it obvious that copper comes from massive stars and type II supernovae or type Ia supernovae. According to Romano & Matteucci (2007) this behavior is a sign of that copper mainly comes from explosive nucleosynthesis in core-collapse supernovae. They also say that the secondary copper contribution comes from the s-process of massive stars. They also say that a sign of the decreasing [Cu/Fe] as [Fe/H] decreases can be described as either be a reduced extent of the weak s-process at low metallicity, or a delayed production from type Ia supernovae. Also, McWilliam & Smecker-Hane (2005) states that this behavior says that it is most probable that copper is created from type II and type Ia supernovae. They also state that a depletion of copper will also result in a depletion of manganese. By looking at the result of manganese

abundances for the exact same stars that this thesis is using, which is done by Battistini & Bensby (2015), one can agree with this. In that article they argue that manganese is thought to be mostly produced by explosive silicon burning in massive stars in their outer incomplete silicon burning layers. Cunha et al. (2002) also has a possibility that, for stars [Fe/H] ≤ -1, the process of silicon burning during type II supernovae is one of the sources for copper. Battistini & Bensby (2015) also argue that this manganese trend seems to disappear as they apply NLTE for manganese.

Due to these trend similarities between manganese and copper these two elements seem like a good comparison, which can be seen in Fig. 3.7, where NLTE correction is not applied manganese. The data for the manganese abundance was taken from Battistini & Bensby (2015). Here one can see that the copper still appear as a rising trend when the metallicity is below -1 dex. For about $-1 <$ [Fe/H] < -0.4 dex the trend is more constant while for metllicity > -0.4 dex the trend is decreasing. This rising trend can be due to, what is said in Simmerer et al. (2003), that copper has two sources: The silicon burning during type II supernovae plus the weak *s*-process that operates during core helium burning.

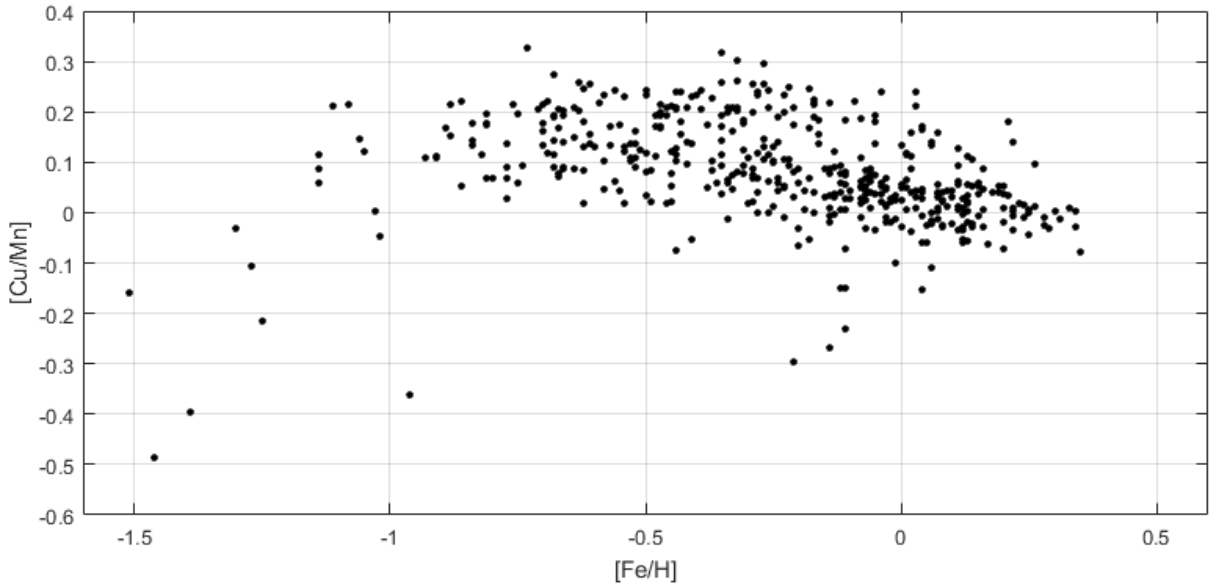

Figure 3.7: A plot of the copper and manganese abundance ratios versus metallicity.

3.1.5 Copper abundance versus α-element abundance

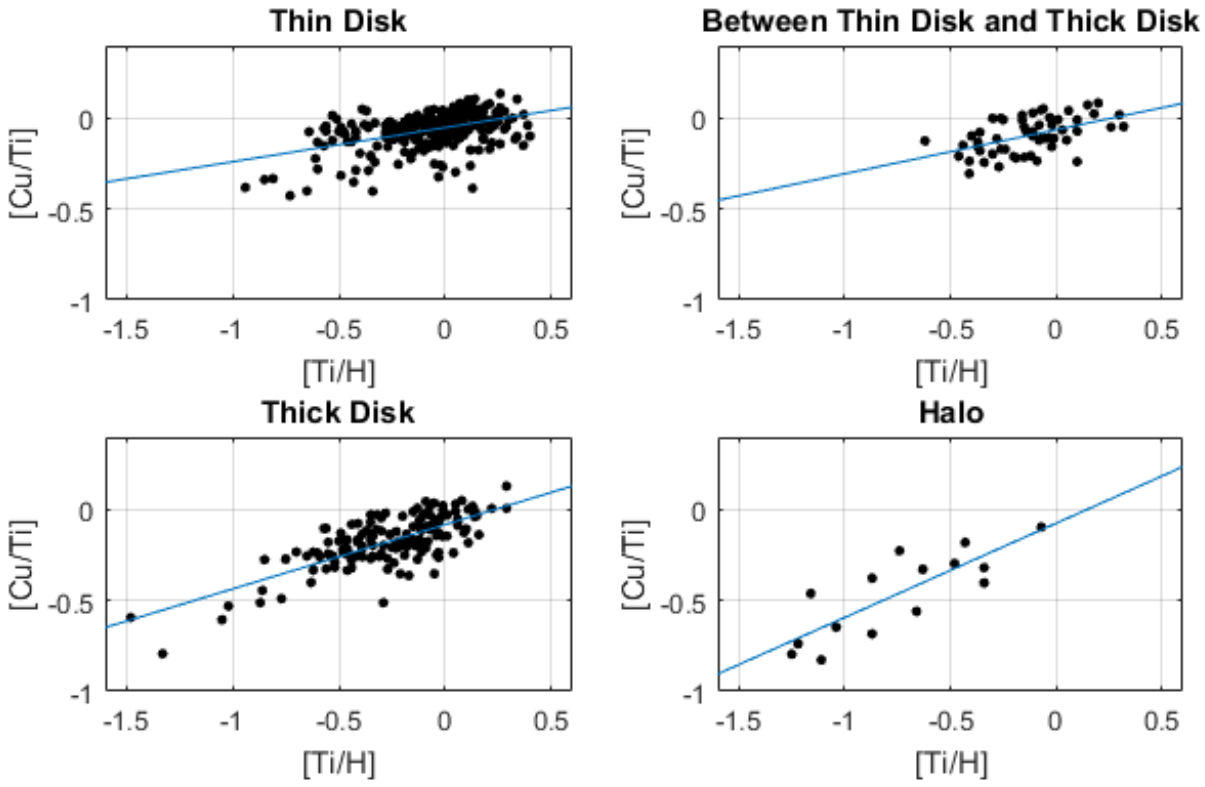

Figure 3.8: Shows plots of the copper and titanium abundance ratios versus titanium abundance. Each plot is separated depending on the orbit of the star around the Milky Way. The lines corresponds to linear fits for all data in each plot.

In Fig. 3.8 we see the ratio in copper and titanium abundance versus the titanium abundance. The plots are separated depending on what orbit around the Galaxy the stars are calculated to have. We can see that there is a constant rising trend throughout the plots. If one takes a look at the individual planes one can see that the trend attempts to be steeper the further away from the galactic plane we get. Since titanium is thought to be mostly produced from type II supernovae for metal poor stars, and copper abundance is increased with titanium abundance, copper must also be produced from type II supernovae. However, the rising trend points out that there should be something more that creates copper or that the creation of copper, in type II supernovae, is somehow metallicity dependent.

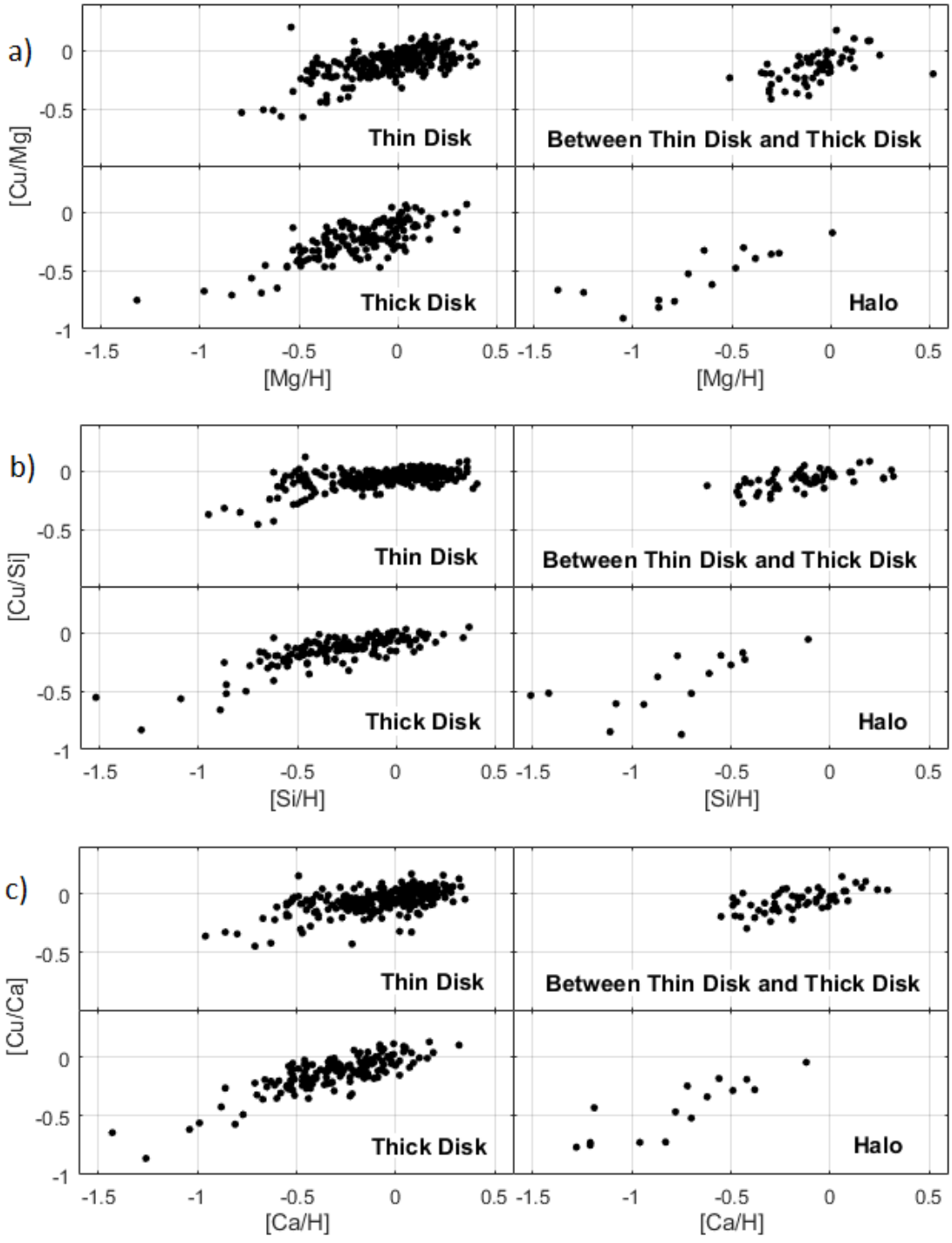

Figure 3.9: Plots of the copper abundance and α-element ratios versus α-elements abundances. In a) Magnesium, b) Silicon and c) Calcium. The stars are divided into the different positions of the Milky Way due to the velocities of the stars.

In Fig. 3.9 one can see the ratio between the copper abundance and the α-elements versus the α-element abundance. One can also see rising trends in all plots. However, in 3.9b and 3.9c, one can observe a bending of the trend around $[\alpha/\mathrm{H}] = -0.6$ dex for the thin and thick disk. In all for $[\mathrm{Fe/H}] < -1$ one can see a flat area. This could be explained by looking at Fig. 6 in McWilliam (1997) which says that these three elements have higher production rate in type II supernovae than titanium, which results in this flat trend for copper. This also means that copper has about the same production rate as these three α-elements in this metal-poor area. Once again one can see that the decreasing trend appears steeper the further out from the galactic plane we get in all plots in Fig. 3.9.

3.1.6 Copper abundance versus age

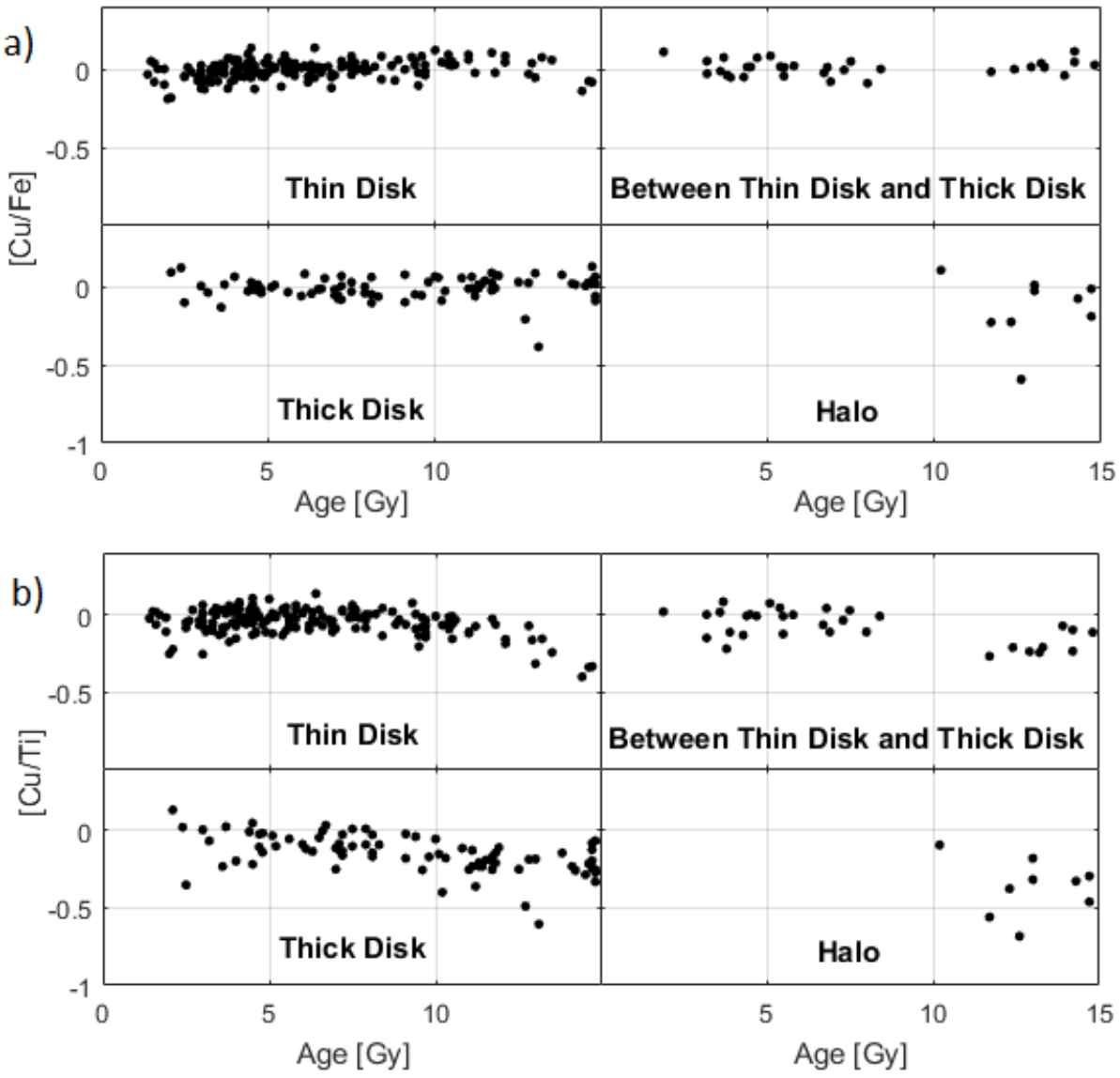

Figure 3.10: Plots of the copper abundance versus age. The stars are divided into the different positions of the Milky Way due to the velocities of the stars. In a) we see copper abundance versus age. In b) we see copper and titanium abundance ratio versus age.

In Fig. 3.10 the stars with an age uncertainty that is >4 Gy are removed to give a clearer result. In Fig. 3.10a we see copper abundance versus age and in Fig. 3.10b we see the copper and titanium abundance ratio versus age. We can see that the copper abundance is

more or less constant except for the halo stars. No specific trends are seen except for that the stars with low copper abundance are also older stars which are more off the galactic plane, according to their velocity. One can also argue that younger stars are more common in the thin disk, while as the stars gets further away from the galactic plane their ages increase. This appearance gives a clear vision why position determination can be valid for age as well. In Fig. 3.10b one can see decreasing trends after about >7 Gy, where the steep of the trend seems to be dependent on where in the star belongs to.

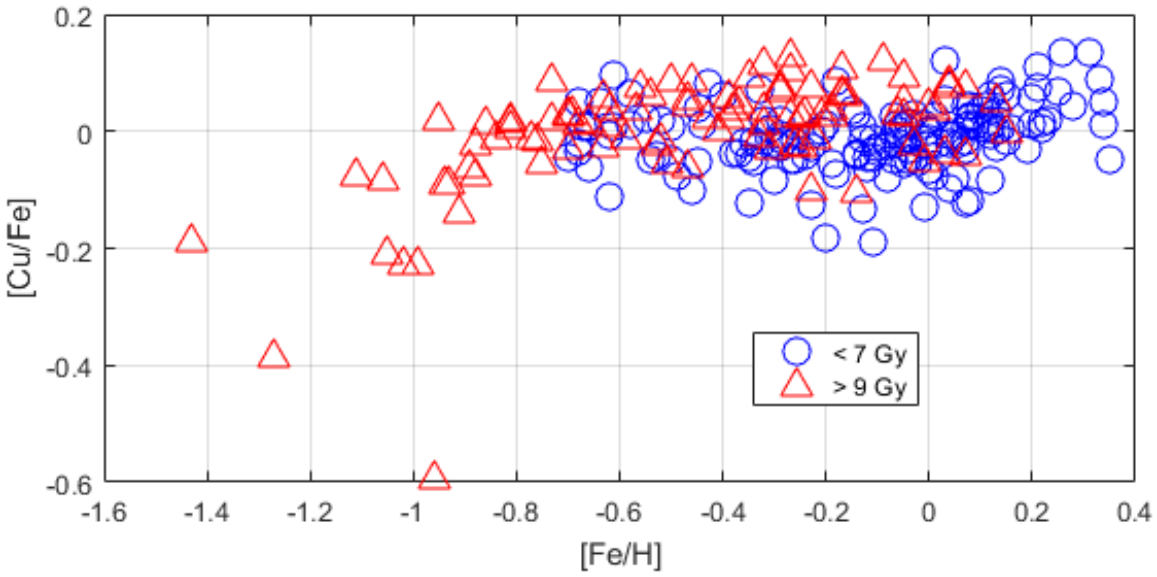

Figure 3.11: The plots represents the copper abundance versus metallicity. The stars are split up into stars younger than 7 Gy, which is shown as blue circles and stars older than 9 Gy, which are shown as red triangles.

The copper abundance versus metallicity, present in Fig. 3.11, here the stars are classified after their age where > 9 Gy are red triangles and if their age is < 7 Gy they are blue circles. The stars with an age in between are removed for a clearer view. The stars that have an uncertainty > 4 Gy are removed, also to give a clearer view. This is chosen after Bensby et al. (2014) and Battistini & Bensby (2016).

The Rising trend between $-1.7 <$ [Fe/H] < -0.6 dex now clearly belongs to the older parts of the Galaxy, when type II supernovae occurred more frequently. However, for -0.6 $<$ [Fe/H] < 0 dex, the age does not seem to matter, the trend is flat. One can argue for this constant to be higher for the thick disk, than for the thin disk. This can be explained due to the different evolution histories in the Milky Way.

As the metallicity increase, for the stars with the age < 7 Gy, and [Fe/H] > 0, the trend once again seems to increase. This increasing trend is not that obvious in Fig. 3.6.

Chapter 4

Conclusions

Through spectral synthesis, the copper abundance has been determined for 491 F and G dwarf stars in the Solar neighborhood. Out of 502 measured stars, 491 gave results that were good enough to be used. Three spectral lines, at 5105 Å, 5218 Å and 5782 Å were used to measure the copper abundance. The spectral line at 5105 Å appeared to not be a very good candidate since about 1/5 of all stars could not be measured with this spectral line, and it appeared that this line only could measure copper abundance in the metallicity range $-1.6 < [\mathrm{Fe/H}] < 0$ dex. The spectral line at 5218 Å was the best one for these spectra, as it could provide most results within the metallicity range of the star sample. The only limitation was for stars with about $[\mathrm{Fe/H}] < -1.6$ dex. The spectral line at 5782 Å had a limit for stars with about $[\mathrm{Fe/H}] < -0.8$ dex. This line also appeared to give a slightly lower result than the other two lines.

This star sample has a metallicity that ranges between $-1.7 < [\mathrm{Fe/H}] < 0.4$ dex. The copper abundance for these 491 ranges between $-0.6 < [\mathrm{Cu/Fe}] < 0.2$ dex.

The result supports the ideas that copper comes from type Ia, type II supernovae and the s-process. The increasing trend, that is seen in all copper abundance plots, makes it clear that type II supernovae must produce copper. Since the trends are increasing, an additional copper producing mechanism must occur, which is the s-process. As the trend appears constant for richer metallicity stars, type Ia supernovae must also be responsible for creation of copper.

To improve this work one can take NLTE into account. As stated by Yan et al. (2015), the results could be affected by up to 0.2 dex for metal-poor stars. Another improvement would be to find some additional spectral lines that can measure stars with $[\mathrm{Fe/H}] < -1.6$ dex, so that these stars also can be taken to account. More spectral lines would also give better statistics for the copper abundance.

Acknowledgment

I would like to extend my utmost gratitude to my supervisor, Thomas Bensby, for his guidance and assistance in making this thesis possible. This work has made use of the VALD database, operated at Uppsala University, the Institute of Astronomy RAS in Moscow, and the University of Vienna.

Bibliography

Asplund, M., Grevesse, N., & Sauval, A. J. 2005, in Astronomical Society of the Pacific Conference Series, Vol. 336, Cosmic Abundances as Records of Stellar Evolution and Nucleosynthesis, ed. T. G. Barnes, III & F. N. Bash, 25

Battistini, C. & Bensby, T. 2015, A&A, 577, A9

Battistini, C. & Bensby, T. 2016, A&A, 586, A49

Bensby, T., Feltzing, S., & Oey, M. S. 2014, A&A, 562, A71

Cunha, K., Smith, V. V., Suntzeff, N. B., et al. 2002, AJ, 124, 379

Gilmore, G. 2004, Science, 304, 1915

Gray, D. F. 2008, The Observation and Analysis of Stellar Photospheres (Cambridge University Press)

Gustafsson, B., Edvardsson, B., Eriksson, K., et al. 2008, A&A, 486, 951

Matteucci, F., Raiteri, C. M., Busson, M., Gallino, R., & Gratton, R. 1993, A&A, 272, 421

McWilliam, A. 1997, ARA&A, 35, 503

McWilliam, A. & Smecker-Hane, T. A. 2005, ApJ, 622, L29

Mishenina, T., Kovtyukh, V., Soubiran, C., Travaglio, C., & Busso, M. 2002, Astronomy & Astrophysics, 396, 189

Prochaska, J. X., Naumov, S. O., Carney, B. W., McWilliam, A., & Wolfe, A. M. 2000, AJ, 120, 2513

Romano, D. & Matteucci, F. 2007, MNRAS, 378, L59

Schwartz, C. 1955, Physical Review, 97, 380

Simmerer, J., Sneden, C., Ivans, I. I., et al. 2003, AJ, 125, 2018

Sneden, C. & Crocker, D. A. 1988, ApJ, 335, 406

Sneden, C., Gratton, R. G., & Crocker, D. A. 1991, A&A, 246, 354

Valenti, J. A. & Piskunov, N. 1996, A&A, 118, 595

Yan, H. L., Shi, J. R., Nissen, P. E., & Zhao, G. 2016, A&A, 585, A102

Yan, H. L., Shi, J. R., & Zhao, G. 2015, ApJ, 802, 36

Appendix A

Line Data from VALD and (Hyperfine Structure source)

Table A.1: A table of the line data used for the spectral line at 5105 Å from VALD3. The hyperfine structure around Cu 1 5105 Å is from Prochaska et al. (2000).

Spec Ion	Wavelength$_{air}$(Å)	log gf	Spec Ion	Wavelength$_{air}$(Å)	log gf
Co 1	5095.0011	-0.781	Ti 1	5100.9639	-1.950
Fe 1	5095.2883	-3.668	Sc 1	5101.1370	-0.561
Ti 1	5095.9610	-1.693	Ti 1	5101.4014	-2.710
Sc 1	5096.7160	-0.580	Fe 1	5101.9718	-2.803
Cr 1	5096.7269	-1.407	Fe 1	5102.2387	-5.163
Ni 1	5096.8629	-0.890	Ti 1	5102.3626	-1.642
Fe 1	5096.9972	-0.268	Cr 1	5102.5277	-2.347
Cr 2	5097.3110	-2.900	Fe 1	5102.6475	-2.057
Fe 1	5097.4821	-1.115	Fe 1	5102.6757	-3.676
Co 1	5098.0527	-1.002	Fe 1	5102.8582	-2.514
Ti 1	5098.3697	-0.485	Ni 1	5102.9659	-2.870
Fe 1	5098.4721	-4.694	Ni 1	5103.0359	-2.501
Fe 1	5098.5722	-0.779	Ti 1	5103.1239	-0.756
Fe 1	5098.6981	-2.026	Co 1	5103.1445	-1.403
Cr 1	5098.9298	-1.246	Ni 1	5103.7635	-2.522
Fe 1	5099.0767	-1.265	Fe 1	5104.0301	-2.870
Sc 1	5099.1810	-0.454	Fe 1	5104.1891	-1.970
Sc 1	5099.2845	-0.076	Fe 1	5104.4372	-1.690
Ni 1	5099.3202	-0.450	Cu 1	5105.505	-3.874
Ni 1	5099.9304	-0.100	Cu 1	5105.509	-2.920
Co 1	5100.0767	-1.089	Cu 1	5105.511	-2.874
Ni 1	5100.4818	-1.851	Cu 1	5105.512	-4.050
Fe 2	5100.6549	-4.170	Cu 1	5105.517	-2.807
Fe 2	5100.8521	-2.172	Cu 1	5105.520	-2.552

Spec Ion	Wavelength$_{air}$(Å)	log gf	Spec Ion	Wavelength$_{air}$(Å)	log gf
Cu 1	5105.531	-2.904	Ti 1	5109.4316	-1.540
Cu 1	5105.536	-2.302	Ti 1	5109.5067	-0.285
Cu 1	5105.558	-2.096	Fe 1	5109.6514	-0.980
Cu 1	5105.503	-4.226	Co 1	5109.7193	-0.999
Cu 1	5105.506	-3.271	Fe 1	5110.2357	-2.119
Cu 1	5105.509	-3.226	Fe 1	5110.3073	-2.160
Cu 1	5105.510	-4.402	Fe 1	5110.3580	-1.366
Cu 1	5105.515	-3.159	Fe 1	5110.4128	-3.760
Cu 1	5105.519	-2.903	Fe 1	5110.4421	-2.367
Cu 1	5105.530	-3.256	Cr 1	5110.7490	-1.320
Cu 1	5105.536	-2.653	Ti 1	5111.0409	-0.675
Cu 1	5105.560	-2.447	Fe 1	5111.3550	-3.287
Cr 1	5105.6006	-2.190	Fe 1	5111.4441	-4.413
V 2	5106.2231	-2.618	Fe 2	5111.6365	-8.197
Fe 1	5106.2390	-1.883	Fe 1	5111.8560	-2.012
Fe 1	5106.4573	-1.687	Cr 1	5112.4840	-3.700
Fe 1	5106.6237	-3.239	Sc 1	5112.8485	-0.458
Sc 1	5107.3579	-0.553	Fe 1	5112.9162	-2.904
Fe 1	5107.4471	-3.087	Cr 1	5113.1250	-1.480
Fe 1	5107.6405	-2.418	Co 1	5113.2227	-2.240
Cr 1	5107.6736	-4.256	Fe 1	5113.2334	-2.407
Fe 1	5108.1601	-3.001	Ti 1	5113.4401	-0.700
Fe 1	5108.1713	-3.746	Ti 1	5113.9099	-2.000
Co 1	5108.2943	-0.921	Fe 1	5114.5097	-2.565
Fe 1	5108.3966	-1.229	Cr 1	5114.9930	-0.297
Fe 1	5108.6143	-2.460	Fe 1	5115.1618	-2.270
Co 1	5108.9007	-0.030	Ni 1	5115.3922	-0.110
Cr 1	5108.9140	-1.991	Fe 1	5115.7767	-2.740
Sc 1	5109.0623	-0.452			

Table A.2: A table of the line data used for the spectral line at 5218 Å from VALD3. The hyperfine structure around Cu 1 5218 Å is from Prochaska et al. (2000).

Spec Ion	Wavelength$_{air}$(Å)	log gf	Spec Ion	Wavelength$_{air}$(Å)	log gf
Cr 1	5208.1000	-1.659	Cr 1	5215.2840	-0.711
Cr 1	5208.4090	0.170	Co 1	5215.4823	-3.351
Fe 1	5208.5787	-4.032	V 2	5215.9326	-2.124
Fe 1	5208.5936	-0.897	Cr 1	5216.1440	-1.306
Fe 1	5208.9592	-4.667	Fe 1	5216.2737	-2.150
Ca 1	5209.5553	-0.867	Ni 1	5216.4778	-1.555
Fe 1	5209.8847	-3.260	V 1	5216.5668	-0.900
Co 1	5210.0385	-1.109	C 1	5217.1015	-1.941
Ti 1	5210.0703	-1.055	Fe 1	5217.3890	-1.070
Fe 1	5210.2767	-1.983	Fe 1	5217.6915	-3.261
Ti 1	5210.3843	-0.820	Fe 1	5217.9148	-2.608
Sc 1	5210.5390	0.433	Fe 1	5217.9189	-1.719
Fe 1	5210.5928	-2.533	Fe 1	5217.9314	-2.837
Cr 2	5210.8242	-3.259	Ni 1	5217.9320	-2.512
Co 1	5210.8304	-0.466	Ti 1	5218.0837	-1.061
Cr 2	5210.8649	-2.941	Cu 1	5218.191	-1.094
Fe 1	5211.2069	-3.436	Cu 1	5218.193	-1.140
Ti 1	5211.2232	-1.950	Cu 1	5218.193	-0.772
Ti 2	5211.5303	-1.410	Cu 1	5218.196	-2.094
Co 1	5211.6902	-0.625	Cu 1	5218.196	-1.027
Co 1	5211.8247	-0.662	Cu 1	5218.196	-0.522
Cr 1	5212.2190	-0.940	Cu 1	5218.202	-2.270
Ti 1	5212.2794	-0.800	Cu 1	5218.202	-1.124
Fe 1	5212.4326	-3.017	Cu 1	5218.202	-0.316
Co 1	5212.6878	-0.110	Cu 1	5218.190	-1.446
Ti 1	5212.9920	-1.160	Cu 1	5218.192	-1.491
V 1	5213.1257	-0.932	Cu 1	5218.192	-1.123
Fe 1	5213.3432	-2.240	Cu 1	5218.196	-2.446
Ti 1	5213.5047	-0.983	Cu 1	5218.196	-1.379
V 1	5213.6469	-1.240	Cu 1	5218.196	-0.874
Co 1	5213.7042	-1.692	Cu 1	5218.202	-2.622
Fe 1	5213.8059	-2.760	Cu 1	5218.202	-1.475
Cr 1	5214.1310	-0.740	Cu 1	5218.202	-0.667
Co 1	5214.4624	-1.105	Ni 1	5218.2565	-2.300
Fe 1	5214.6066	-2.242	Fe 2	5218.3324	-3.386
Cr 1	5214.6130	-1.087	Fe 1	5218.5040	-2.600
Co 1	5214.7450	-0.444	Ca 1	5218.5293	-0.790
Cr 1	5214.9012	-1.069	Co 1	5219.0047	-0.948
Fe 1	5215.1800	-0.871	Si 1	5219.1415	-3.046

Spec Ion	Wavelength$_{air}$(Å)	log gf	Spec Ion	Wavelength$_{air}$(Å)	log gf
Sc 1	5219.6255	0.363	Cr 1	5224.5330	-1.503
Ti 1	5219.6342	-1.846	Ti 1	5224.5400	-0.280
Ti 1	5219.7015	-2.220	Cr 1	5224.5830	-1.970
Cu 1	5220.0659	-0.590	Cr 1	5224.9250	0.070
Fe 2	5220.0757	-8.217	Ti 1	5224.9300	-0.070
Fe 1	5220.2090	-3.460	Cr 1	5225.0200	-0.300
Ti 1	5220.2587	-1.520	Ni 1	5225.1130	-1.452
Ni 1	5220.2905	-1.310	Fe 1	5225.5260	-4.789
Cr 1	5220.8910	-0.890	Fe 1	5225.5345	-2.518
Fe 1	5221.0353	-1.684	V 1	5225.7241	-0.510
Fe 1	5221.1725	-3.594	Cr 1	5225.8130	-1.500
Fe 1	5221.4313	-7.059	Fe 1	5226.0630	-4.458
Cr 1	5221.7510	-0.349	Ti 2	5226.5384	-1.260
Fe 1	5221.7596	-3.617	Fe 1	5226.8612	-0.555
Fe 1	5222.3944	-3.835	Fe 1	5226.8962	-1.906
Co 1	5222.4877	-0.547	Cr 1	5226.9000	-1.536
Cr 1	5222.6670	-1.410	Cr 1	5227.0670	-1.636
Ti 1	5222.6743	-0.621	Fe 1	5227.1495	-1.352
Fe 1	5222.8937	-2.610	Fe 1	5227.1889	-1.228
Fe 1	5223.1824	-1.783	Fe 2	5227.4854	0.846
Fe 1	5223.5263	-2.864	Fe 1	5227.4964	-1.819
Cr 1	5223.5907	-1.275	Fe 1	5227.5177	-2.511
Ti 1	5223.6200	-0.490	Fe 2	5227.5871	-2.239
Cr 1	5223.8770	-1.143	V 2	5227.7101	-2.360
Cr 1	5224.0640	-0.870	Cr 1	5227.7320	-2.050
Fe 1	5224.0790	-2.414	Ti 2	5227.8730	-2.961
Fe 1	5224.1200	-2.907	Cr 1	5228.0860	-2.112
Ti 1	5224.1369	-2.728	Fe 1	5228.1065	-3.173
Fe 1	5224.2983	-4.080	Fe 1	5228.3753	-1.290
Ti 1	5224.3000	0.130	Fe 1	5228.9592	-3.942
Fe 1	5224.4470	-2.568			

Table A.3: A table of the line data used for the spectral line at 5218 Å from VALD3. The hyperfine structure around Cu 1 5782 Å is from Prochaska et al. (2000).

Spec Ion	Wavelength$_{air}$(Å)	log gf	Spec Ion	Wavelength$_{air}$(Å)	log gf
Si 1	5772.0272	-3.107	Cu 1	5782.066	-3.445
Si 1	5772.1460	-1.750	Cu 1	5782.078	-2.746
V 1	5772.4119	-0.550	Cu 1	5782.106	-2.746
Cr 1	5772.6658	-1.597	Cu 1	5782.117	-2.746
Fe 1	5773.4493	-3.826	Cu 1	5782.170	-2.299
Ti 1	5774.0268	0.480	Cu 1	5782.053	-3.496
Fe 1	5774.2563	-3.281	Cu 1	5782.062	-3.797
Ti 1	5774.4761	-2.020	Cu 1	5782.074	-3.098
Ti 1	5774.6638	-0.596	Cu 1	5782.105	-3.098
Fe 1	5774.9150	-3.385	Cu 1	5782.117	-3.098
Fe 1	5775.0802	-1.298	Cu 1	5782.173	-2.651
Fe 1	5776.2240	-3.331	V 1	5782.5982	-2.140
V 1	5776.6874	-1.540	Cr 1	5783.0650	-0.500
Fe 1	5777.6501	-3.160	Cr 1	5783.1100	-1.746
Cr 1	5777.7490	-1.324	V 1	5783.5014	-0.246
Si 1	5777.8455	-3.349	Cr 1	5783.8500	-0.295
Fe 1	5778.4526	-3.430	Fe 1	5783.8933	-3.462
Fe 1	5778.8087	-3.177	Fe 1	5783.9197	-4.639
Fe 1	5779.5557	-2.374	V 1	5784.3648	0.134
Fe 1	5779.6877	-2.085	Cr 1	5784.6001	-1.915
Mn 1	5780.1612	-0.928	Fe 1	5784.6576	-2.532
C 1	5780.2063	-1.048	Cr 1	5784.7125	-2.626
Fe 1	5780.2828	-3.420	Cr 1	5784.9690	-0.380
Si 1	5780.3838	-2.350	Fe 1	5785.2699	-1.088
Fe 1	5780.5994	-2.640	V 2	5785.6335	-2.299
C 1	5780.6776	-0.462	Ti 1	5785.6519	-0.078
Ni 1	5780.7287	-2.637	Fe 1	5785.6570	-1.706
Ti 1	5780.7609	-1.210	Cr 1	5785.7350	-0.581
Fe 1	5780.8036	-2.918	Cr 1	5785.9161	-3.965
Cr 1	5780.9050	-1.299	Cr 1	5785.9453	-4.131
Cr 1	5781.1670	-1.000	Ti 1	5785.9761	0.600
Cr 1	5781.1790	-0.854	V 1	5786.1224	-0.114
Fe 1	5781.3712	-1.994	V 1	5786.1559	0.014
Fe 1	5781.4909	-3.287	Fe 1	5786.5307	-1.925
Y 2	5781.6879	-1.390	Cr 1	5787.0210	-1.591
Cr 1	5781.7510	-0.726	Fe 1	5787.2626	-4.130
Fe 1	5782.0774	-3.391	Si 1	5787.2840	-1.845
Fe 1	5782.1109	-1.710	Cr 1	5787.9190	-0.083
Cu 1	5782.059	-3.144	Fe 1	5787.9669	-3.078

Spec Ion	Wavelength$_{air}$(Å)	log gf	Spec Ion	Wavelength$_{air}$(Å)	log gf
Fe 1	5788.0849	-3.615	Cr 1	5790.9570	0.244
Cr 1	5788.3810	-1.490	Fe 1	5791.0169	-2.234
V 1	5788.5916	-1.144	Fe 1	5791.1920	-2.070
Si 1	5788.9841	-1.312	Ti 1	5791.2742	-0.702
Si 1	5789.1474	-1.963	Fe 1	5791.5235	-1.894
Ti 1	5789.7462	-0.474	Cr 1	5791.7550	-0.987
Fe 1	5790.4078	-2.107	Cr 1	5792.1730	-4.478
Cr 1	5790.6510	-3.916			

Appendix B

Bad lines

Table B.1: This is a table of the stars where the spectral line at 5105 Å was too bad to be taken into account.

Id of star (HIP)	Id of star (HIP)	Id of star (HIP)	Id of star (HIP)
305	44821	86193	105790
2743	45514	86694	106006
5817	46685	87679	106678
6177	50274	88010	106931
6856	53719	88631	108598
7080	58401	89554	109012
7091	59639	89881	109207
8572	60462	90151	110084
9316	60632	90365	110468
10977	64706	90539	110843
13388	68464	90896	111312
13848	72479	91360	111978
14023	72688	91471	112243
22632	73444	91582	113777
24819	74234	93186	114460
27080	74235	93507	114743
27910	74537	96425	114761
28369	76976	96881	114962
34028	80043	98020	115577
35718	80700	98964	115861
35750	81952	102580	117526
36269	82265	103609	117902
37171	84781	103692	
38625	84907	105521	
43393	85320	105606	

Table B.2: This is a table of the stars where the spectral line at 5218 Å was too bad to be taken into account.

Id of star (HIP)	Id of star (HIP)	Id of star (HIP)
8572	68727	87101
36269	72797	88010
50834	73385	89554
54641	74234	93186
60632	76976	114761
68464	86694	114962

Table B.3: This is a table of the stars where the spectral line at 5782 Å was too bad to be taken into account.

Id of star (HIP)	Id of star (HIP)	Id of star (HIP)
8572	59699	87101
18802	60632	88010
27128	68464	89554
34285	68727	91089
36269	73385	93186
36849	73444	98020
47048	74079	98532
51028	75023	98565
54641	76976	100394
56664	78267	102046
57360	83867	114761
58145	86694	114962
59490		